EUR 4951 e

COMMISSION OF THE EUROPEAN COMMUNITIES

MIGRATION OF FISSION PRODUCTS IN NEAR ISOTROPIC PYROCARBON
Final Report

by

B. CHINAGLIA, G. MOSCA and H. WALTHER (SORIN)

1973

EUR 4951 e

MIGRATION OF FISSION PRODUCTS IN NEAR ISOTROPIC PYROCARBON
Final Report by B. CHINAGLIA, G. MOSCA and H. WALTHER

The migration of Ba, Xe, Zr and Cs atoms in pyrocarbon has been measured in the range of temperature between 1200^{0} C and 1800^{0} C. The pyrocarbon samples were of different types and origin and were characterized by X ray analysis. Rather large variations of apparent diffusion constants have been measured for the examined fission products among the various pyrocarbon types. No definite correlation has been found between the diffusion constants and the structural parameters. It is suggested that revised diffusion models and improved microstructural characterization are needed for a better description of the atomic transport in pyrocarbon.

EUR 4951 e

MIGRATION OF FISSION PRODUCTS IN NEAR ISOTROPIC PYROCARBON

Final Report

by

B. CHINAGLIA, G. MOSCA and H. WALTHER (SORIN)

1973

ABSTRACT

The migration of Ba, Xe, Zr and Cs atoms in pyrocarbon has been measured in the range of temperature between 1200° C and 1800° C. The pyrocarbon samples were of different types and origin and were characterized by X ray analysis. Rather large variations of apparent diffusion constants have been measured for the examined fission products among the various pyrocarbon types. No definite correlation has been found between the diffusion constants and the structural parameters. It is suggested that revised diffusion models and improved microstructural characterization are needed for a better description of the atomic transport in pyrocarbon.

KEYWORDS

Index

1. Introduction

The migration of fission products through protective car bon coatings and their escape from fuel elements is an important process affecting the ultimate performance of High Temperature Gas Cooled Reactors.

Many experimental studies have been performed regarding the escape of some gaseous or solid fission products /1/ /2/ /3/ from graphite matrices in various forms (powders, compacts); from the experimental results it appears that only in few cases simple diffusion laws applied to the physical configuration under consideration can describe the migration process.

Fast and slow diffusion, trapping mechanisms, surface com pound formation have been postulated to interpret the experi mental results.

Furthermore there is scarce information about the dependence of the measured diffusion properties upon the graphite structure.

The situation is perhaps more complex when pyrolytic carbon (PyC) is considered. PyC coatings for fuel particles must act as a barrier for fuel and fission product escape, but this latter is a very complicated process within the severe operating conditions of a reactor core: neutron and fission-fragment damage, fission gas pressure, microstructur al changes due to temperature may cause the rupture of the coating and the escape of the activity almost independently of the diffusion properties of the coating material. For this reason much work has been devoted to irradiation tests

in order to select among the wide variety of PyC structures those ones which can withstand operating conditions without ruptures.

The importance of the escape from intact coatings by diffusion is however now being increased by the successful development of coating structures of high mechanical stability and low contamination, but it is generally difficult to interpret the above irradiation tests in terms of diffusion properties. Furthermore some important parameters often have not been well defined (for instance the level and distribution of contamination of fissile elements within the coating, or the PyC structure).

Existing data on diffusion coefficients of fission products in PyC are rather scarce /4/ /5/ /6/; by comparison with the better known coefficients of actinide elements in PyC /7//8/ /9/ it may be expected that large variations may be found in the diffusion properties, depending on some structural parameters which are however not well known; in particular it is not well established if the same parameters which have revealed useful for correlating mechanical properties changes (namely: density, anisotropy, crystallite size and c spacing) are still apt to determine univoquely the diffusion behaviour of PyC.

From the above considerations it seems useful for the prediction of activity escape from fuels to investigate in more detail the diffusion problem in PyC, having in mind that for a complete description of the process one should determine:

- the physical law controlling the process

- the values of the constants which appear in the mathemat ical model approaching such a physical law

- the structural parameters upon which the constants are dependent.

The present study is mainly concerned with the effect of the structure of PyC on the diffusion of four representative fission products: Xe, Ba, Zr, Cs perpendicular to the depo sition planes.

The range of variations of the structural parameters has been limited to those values which can be considered realistic from the point of view of dimensional changes and ruptures, namely:

- BAF $\sqrt{10}$: 1 ÷ 1.3

- Density : $(1.5 ÷ 2.0) g/cm^3$

- Crystallite size L_c : ∼ $(50 ÷ 100)$ Å

Two experimental techniques have been used. In the first (applied to Xe, Zr, Ba) the initial condition is a step di- stribution of fission fragments obtained by recoil. The second technique makes use of a constant potential source and has been applied to Cs diffusion.

2. Experimental

2.1. Specimens

The specimens used in this work are coming from three different origins; in any case they have been prepared by coating in a fluidized bed graphite disks of dimensions of about 0.7 mm thickness and 7 mm diameter.

The list of samples examined in the present study is shown in Table I, together with the deposition conditions and the structural parameters

Samples (A) and (B) have been obtained from other labora tories ; samples S have been coated at SORIN.

The optical structure (Table I) is determined from the appearance of the PyC when a metallographic specimen is ob served under polarized light:

- "Columnar" indicates a structure with large growth cones

- "Isotropic" indicates a structure without distinct grains and not optically active, in accordance with the termino-logy of Bokros /11/

Some examples are given in Fig. 1

For the successful application of the subsequent diffu-sion measurements, the samples must possess some special characteristics: sufficient PyC thickness, flat surface, absence of U contamination. Specimens S have been prepar

ed with special care in order to meet these requirements:
the supporting graphite disks were prepared with rounded
off edges which eliminate the growth of concave surfaces.

The contamination usually is coming from fuel particles
coated together with the disks; in our case during the
coating process the furnace contained particles with inert
(MoC_2) kernel and the contamination was avoided.

For the other samples activation analysis and micagraphs
revealed in some cases troublesome amounts of uranium: in
these cases solid fission product diffusion could not be per
formed.

2.2. Step initial distribution

The used techniques is the same, with minor changes, as
described in a previous work /4/.

One face of the disk is worked with grind paper and dia
mond paste (0.1 μm) on a lapping plate until a flat surface
is obtained. The worked face is put in contact with a thin
U layer deposited on aluminum and the couple irradiated
with neutrons. Usually the U layer was of ~ 0.2 mg/cm^2,
with 90% enrichment in U^{235}; the deposition on Al was per
formed by electrolysis according to the procedure describ-
ed by Laul /12/.

---

* " Micagraph" is the name for a technique set up in this labo-
ratory for measuring. the distribution of fissile elements in
coatings; this technique makes use of the detection of the
fission fragment tracks in a foil of mica irradiated in con-
tact with a section of a specimen.

During irradiation about one half of the produced fis sion fragments enter the PyC and produce a step distribu tion for a depth equal to the range and a tail due to straggling effects. The detailed shape of the distribution is given in Ref. 4.

After irradiation PyC and aluminum U target are separated and their La^{140} activities measured with a γ spectrometer in standard conditions. The following information is obtained:

- The ratio r_i between the activity recoiled into the specimen i and the activity recoiled in aluminum plus the activity remained in the U layer. If the thickness of the U layer is t, and R represents the range of the fis sion fragment under consideration in uranium, then:

$$r = \frac{2R-t}{2R+t}$$

Since r refers to Ba^{140} activity, in which case R $\approx$ 10 mg/cm^2, the value of r expected from the uranium weight is $\sim$ 0.99. Disks giving r values outside (0.96÷1.00) were not used for subsequent diffusion; lower values would indicate thicker uranium layers (actually not uni form deposits) and higher values inner PyC contamination: in both cases the initial distribution would be different from the expected curve.

- The total amount of fission products within the PyC; this is easily calculated from the counting rate C of the peak at 1.6 MeV of La^{140} in known counting conditions. The total amount of fission products, i.e. the number

of f.p. atoms within the PyC, is then given by:

$$N.F.P. = 2 \cdot \frac{C}{\varepsilon \cdot F(t,\tau) \cdot y \, \lambda_1}$$

where:

ε = detection efficiency

$F(t,\tau)$ = time factor depending on irradiation time τ and decay time t

$$\approx \frac{e^{-\lambda_1 t}}{\lambda_2 - \lambda_1} \lambda_2 \qquad (\lambda_1 t \ll 1, \quad \lambda_2 \tau \gg 1)$$

y = fission yield for 140 mass chain
$$= 5,8 \cdot 10^{-2}$$

λ_1 = decay constant of Ba^{140} = $5,42 \cdot 10^{-2}$ d^{-1}

λ_2 = decay constant of La^{140} = $0,415$ d^{-1}

The mean concentration ν (number of f.p.'s per unit PyC volume) obtained during the experiments in the initial distribution is:

$\nu \simeq 2 \cdot 10^{17}$ f.p.'s/cm^3, corresponding to

about $\qquad 1 \cdot 10^{-6}$ (g of Zr, or Ba, or Xe)/(g of PyC)

or $\qquad 1 \cdot 10^{-7}$ (atoms of Zr, or Ba, or Xe)/atom of C.

- The ratio $r_{i/M}$ between the activity of each specimen i and the activity of an aluminum uranium target taken as monitor for all the specimens of a given irradiation. Actually two or more monitors are used; one of them consists of a small piece (about 1/10) of a target and is used for the calibration of the xenon counter as explained below.

The subsequent experiments are different for xenon and for solid fission products.

In the first case it is possible to determine the dif fusion coefficient from the rate of escape as a function of annealing time, whilst in the second case it is neces sary to measure the internal profile after diffusion in addition to the escaped fraction.

The difference results clearly from the analytical de scription of section 3, where the escape is dependent on 2 processes (evaporation and diffusion): in the case of xenon the evaporation coefficient may be assumed infinite and the escape is controlled only by the diffusion coeffi cient.

2.2.1. Isothermal diffusion anneal: xenon diffusion

This is performed in a furnace whose scheme is shown in Fig. 2. A graphite crucible extending up to the top of the furnace is heated by a graphite resistance. Elec trical power is supplied by means of a control transfor mer which maintains constant power and costant tempera- ture (the heat losses being constant) as was checked in a series of tests: maximum temperature variations were of ± 5°C at 1.600°C. Helium gas, previously purified in a trap filled with molecular sieve and cooled with liquid nitrogen, flows through small holes at the bottom of the crucible and is sent to a charcoal trap cooled with liquid nitrogen. Inside the crucible the helium pressure is about 1 cm Hg.

When the crucible is at the wanted temperature, as
determined with an optical pyrometer through a quartz
window, the specimen, which was previously inserted in
a glass tube ending over the crucible as shown in Fig. 2,
is moved by means of a magnet and drops in the crucible.
Since the mass of the specimen is very low, the specimen
attains in a very short time (less than 1 minute) the
crucible temperature and the starting time for diffusion
may be known with high precision.

During the anneal the active gases escaping from the
sample are swept by the stream of helium and collected
in the charcoal trap.

A NaI(Tl) crystal faced to the trap records the acti
vity as a function of time. The detector dimensions
(1" diameter, 3 mm thickness) and the electronic bias
are chosen for optimum counting of Xe^{133} activity (ener
gy of γ emission 80 keV) in presence of the background,
and of the other gamma lines.

In order to convert the xenon counting rate $C_{Xe}(i)$ of
sample i in released fraction, a calibration is neces-
sary.

This is performed by melting in the same furnace and
in the same measuring conditions an aluminum monitor M,
loaded with fission products having a total activity
about 1/10 of the total activity of the sample. When
the monitor is dropped in the crucible at temperatures
in excess to the Al melting point ($\sim 660^{\circ}C$), the Xenon
trap counting rate increases suddenly and attains in few
minutes its final value $C_{Xe}(M)$ indicating that (a) the

transit time from emission to collection is very short (less than 1 minute for reaching 90% of final value) and (b) that all the Xe-activity has been released.

The fraction f of activity released from sample i is then given by:

$$f = \frac{C_{Xe}(i)}{C_{Xe}(M)} \, e^{+\lambda\left[t_i - t_M\right]} \cdot \frac{1}{r_{i/M}} \tag{2.1}$$

where:

$t_i - t_M$ = decay time between diffusion of sample i and melting of monitor M

λ = 0.131 d^{-1} (Xe^{133} decay constant).

This procedure is not based on absolute calculations but on relative measurements and therefore can give a good accuracy.

Since accidental errors might arise from possible variations of the trap-detector geometry, this calibration has been repeated every 3 or 4 diffusion runs, and in addition after each diffusion or calibration the trap was removed and its activity measured also with a larger detector in geometry conditions less dependent on the above effects.

The analysis of the calibration runs shows that the relative standard deviation of the whole procedure is about 10%, and this may be assumed as the error in the determination of f for xenon.

2.2.2. Barium and zirconium

In this case, as well for other solid fission products it is necessary to have a measurement of the internal concentration profile after annealing and this requires sectioning thin layers. The technique used is the following: the specimen is pressed against emery paper sup ported by a flat plane, and then uniformly moved for a length of about 20 cm and at the same time slowly rotated.

Actually this abrasion is performed with the mechanic al apparatus shown in Fig. 3: the paper strip is support ed by a glass plate; the sample is pressed by means of a piston whose axis is normal to the glass plate; elastic rubber between the piston and the PyC disk assures friction and compensates small variations in the specimen thickness; the pressure is applied by means of loads on the piston and this is connected to a rigid frame moving on wheels and motor driven; the slow rotation (1 revolution/10 cm) is performed by hand. Typical working con ditions are: load 0.4 Kg, paper 2/0, thickness removed $\sim 10\,\mu$m in 20 cm. Prior and after any abrasion the sample is weighed and its thickness measured with a micrometer (sensitivity 1 μm) at 5 positions.

The paper strip is covered with adhesive tape and its activity measured; if, after the activity measurement, it appears that the thickness abraded is too large to give a detailed shape of the concentration profile, the strip is cut in more sections, each one corresponding to a thickness proportional to its length; this assumption

has been verified with specimens with uniform activity concentration (the initial distribution).

Conventional spectrum stripping techniques have been used to analyze γ ray spectra for the determination of the activity of various fission products. However since the diffusion coefficients are quite different and the thickness available is quite small, it is not possible to have in a single specimen concentration profiles relative to more than one fission product with a shape useful for subsequent interpretation.

It was rather fortuitous that the annealing time used for xenon gave a measurable diffusion of Zr, so that almost all the specimens already annealed for xenon were also analyzed for zirconium. In the case of barium it was necessary to repeat the diffusion anneals with much shorter times (by a factor $\sim$ 100). Other fission product (for instance cerium) which were initially detected, were not considered because their migration was intermediated between Ba and Zr and would have required intermediate annealing times. The problem of γ ray spectra analysis was therefore much reduced because in any specimen only a single activity was to be measured.

The details of the measurements are the following:

Barium

In the case of barium its daughter activity La^{140} is measured. This procedure greatly simplified the determination of Ba activity since the 1.6 MeV peak of La^{140} is usually well resolved in a γ spectrum of fission products with decay time within 1 ÷ 2 months, but requires

a waiting time after the diffusion anneal in order to
restore the Ba-La equilibrium. The equilibrium condition
is determined by measuring the decay of the activity re-
maining in the specimen. It has been found that during
diffusion the escape of La is much lower than the escape
of Ba; in this case the true fraction f_r of Ba remaining
in the sample is given by:

$$f_r = (f_{r,m} - e^{-\lambda^* t}) \frac{1}{(1 - e^{-\lambda^* t})} \qquad (2.2)$$

where:

$f_{r,m}$ = measured fraction at time t after annealing

$\lambda^* = \lambda_{La} - \lambda_{Ba} = 0.36 \ d^{-1}$

and the equilibrium condition is given by:

$f_{r,m} \gg e^{-\lambda^* t}$ (for instance $f_{r,m} \geq 100 \cdot e^{-\lambda^* t}$).

Some difficulties may arise during the γ measurement
of the first PyC layers, because near the surface the
Ba concentration is usually much lower than that of the
other fission products and the peak at 1.6 MeV may be
masked by a background arising from the pile-up of inten
se γ lines of lower energy. To avoid this background in
some cases the γ detector was covered with a 6 mm lead
absorber which reduces the low energy radiation more than
the 1.6 MeV γ line.

Zirconium

Zirconium is measured from the γ activity at 0.76 MeV; actually in a NaI(Tl) spectrum the peak at this energy is made of three components: 0.724 and 0.756 MeV from Zr^{95} and 0.765 from its daughter Nb^{95}. Therefore also in the case of Zr it is necessary to wait for equilibrium between Zr and Nb after annealing. Spectra taken with a high resolution Ge/Li detector have permitted to verify that under the used conditions (decay time greater than 6 months after annealing) the equilibrium was reached.

2.3. Constant potential source

This technique is analogous to that described by Zumwalt $\underline{/5/}$: the disks are annealed inside a sealed tantalum cruci ble containing graphite powder tagged with Cs^{134} (in the form of cesium chloride). After annealing the edges of the disk are removed and the specimens are then processed as described in the previous section to get internal profile of cesium atoms diffused from the external constant source.

3. Models for diffusion and mathematical solutions

The diffusion in PyC is certainly a very complex phenomenon and a full description would require a correspondingly compli-cated model and mathematical computations which are outside the scope of the present work. A reasonable procedure when experimental data are to be interpreted is to adopt the simplest

model which fits the results, and to determine the parameters controlling the process according to the model.

In the following some migration and escape models are considered. For the first ("Diffusion and evaporation") mathematical solutions relative to the geometry of the experiments have been derived and used for the determination of the diffu sion constants. It has been found that this model can describe most of the data, although some discrepancies indicate that also the effects listed in the other models play an important role on the process.

a) Diffusion and evaporation

The movement of atoms inside the solid is assumed to occurr according the classical diffusion law:

$$\frac{\partial c}{\partial t} = D \cdot \nabla^2 c$$

where c is the concentration; the solid is thought homo geneous but not necessarily isotropic and the only driving force for atom movement is the concentration gradient. At the surface the diffusing atoms may evaporate; since during the experiment the concentration outside the specimen is effectively zero, the appropriate boundary condition is:

$$D \cdot \frac{\partial c}{\partial x} = E \cdot c$$

where x is the coordinate normal to the surface, and E the evaporation coefficient.

In our case the PyC disk has been approximated to an in finite slab. We consider firstly the case of an isotropic solid.

When an infinite half space $(x > o)$ is considered, with the initial condition

$$c = c_0 \qquad x < R \qquad \text{for} \qquad t = o$$

$$c = 0 \qquad x \geqslant R \qquad \text{for} \qquad t = o$$

the appropriate solutions are:

$$\frac{c}{c_0} (x,t) = \text{erf} \frac{x}{2\sqrt{\tau}} - 0.5 \text{ erf} \frac{x-R}{2\sqrt{\tau}} - 0.5 \text{ erf} \frac{x+R}{2\sqrt{\tau}}$$

$$(3.1)$$

$$+ e^{Fx+F^2\tau} \text{erfc} \left(\frac{x}{2\sqrt{\tau}} + F\sqrt{\tau}\right) - e^{F(x+R)+F^2\tau} \text{erfc} \left(\frac{x+R}{2\sqrt{\tau}} + F\sqrt{\tau}\right)$$

$$f = \frac{\text{ESCAPED}}{\text{TOTAL}} = 1 - \frac{e^{F^2\tau + FR}}{FR} \text{erfc} \left(\frac{R}{2\sqrt{\tau}} + F\sqrt{\tau}\right)$$

$$(3.2)$$

$$- \left(1 + \frac{1}{FR}\right) \text{erf} \frac{R}{2\sqrt{\tau}} + \frac{2\sqrt{\tau}}{\sqrt{\pi}R} \left(1 - e^{-R^2/4\tau}\right) + \frac{e^{F^2\tau}}{FR} \text{erfc} \left(F\sqrt{\tau}\right)$$

where $F = \frac{E}{D}$, $\tau = Dt$ and f is the escaped fraction.

If the evaporation coefficient is very large compared to D the solutions are

$$\frac{c(x,t)}{c_0} = \text{erf} \frac{x}{2\sqrt{\tau}} - 0.5 \text{ erf} \frac{x+R}{2\sqrt{\tau}} - 0.5 \text{ erf} \frac{x-R}{2\sqrt{\tau}} \qquad (3.3)$$

$$f = \frac{2\sqrt{\tau}}{\sqrt{\pi} \cdot R} \left(1 - e^{-R^2/4\tau}\right) + \text{erfc} \frac{R}{2\sqrt{\tau}} \qquad (3.4)$$

as can be verified by letting F tend to infinity in (3.1)
and (3.2), or more directly, using the boundary condition:

$$c(o,t) = 0 \qquad t > o$$

When $\tau \ll 1$, the well known approximation of (3.4) is:

$$f = \frac{2\sqrt{\tau}}{\sqrt{\pi} \cdot R} \qquad (3.5)$$

valid up to $f \lesssim 0.2$.

As shown in the Appendix in some cases the solution (3.1)
can be approximated by:

$$\frac{c(x,t)}{c_o} = \frac{e^{-x^2/4\tau}}{\sqrt{\pi}} \cdot Q(x,t) \qquad (3.6)$$

where $Q(x,t)$ is nearly constant.

This result simply reflects the fact that for deep pe-
netrations and long diffusion times, the step initial di-
stribution is equivalent to an instantaneous source[*].

The above solutions have been computed for a large ran
ge of values.

For xenon equation (3.5) can be directly applied to de
termine D from the slope of the measured fractional release
f versus $\sqrt{t}$.

For Zr (and Ba when $f \ll 1$) the conditions for the vali-
dity of (3.6) can be usually met;   the value of D can

---

[*]

The instantaneous source is defined by initial condition
$c = c_o$ for $t = 0$, $x = 0$.

then easily be found from the slope of $\ln c$ versus x^2.

In the other cases the experimental curve should be fitted by a calculated one with the appropriate couple of values of F and τ. For selecting as a first approxi_ mation this couple of values, the measured quantities f and $\bar{x}$ are used; $\bar{x}$ is defined as the value of x at which the integral of the concentration is one half the initial value:

$$\int_0^{\bar{x}} c(x,t)\,dx = \frac{1}{2} \int_0^{\infty} c(x,t)\,dx \quad .$$

The values of f and $\bar{x}$ are easily measured; the lat_ ter one is obtained from an integral curve in which the ac_ tivity remaining in the sample after each abrasion is plot_ ted against the thickness.

Numerical values of $\bar{x}$ and f have been computed for several values of τ and F, obtaining the graph of Fig. 4.

From these curves, the $\bar{x}$, f values give at once the F, τ couple.

For the cesium experiment the initial and boundary con_ ditions are:

$$c = 0 \qquad x > 0; \qquad t = 0$$

$$c = c_0 \qquad x = 0 \qquad t \geqslant 0$$

In this case the solution is:

$$\frac{c}{c_0} = \text{erfc}\,\frac{x}{2\sqrt{Dt}} \tag{3.7}$$

b) Grain boundary diffusion

This problem has been considered by Fisher $\underline{/13/}$, Whipple $\underline{/14/}$ and Suzuoka $\underline{/15/}$ for an idealized case in which the grain boundary is an infinite isotropic slab parallel to the diffusion direction x.

The model has been modified for polycrystalline materials by Suzuoka and by Levine and Mac Cullum $\underline{/16/}$.

Their solutions differ depending on the different simplifying assumptions, but a relevant feature is that ln c (x,t) is proportional to x (or to $x^{6/5}$) for both cases of constant and instantaneous source. Physically the grain boundary acts as a high diffusivity path along which the concentration is nearly constant during much of the anneal, and from which the solute is drained in the surrounding grains. If the dimensions L of these latter are much greater than the penetration distance inside the grain, i. e. if L $\gg \sqrt{D_1 t}$ where D_1 is the lattice diffusion coefficient and t the annealing time, the physical configuration approaches the assumptions in the above models. In this case a graphical method and the Whipple solution can be used to deduce from the experimental c(x,t) versus x curve the values of D_1 and D_g (the grain boundary diffusion coefficient).

This method is described in some detail since it has been applied to some curves of Cs diffusion in the present work.

The concentration is expressed as follows:

$$c(x,t) = c_1 + c_2$$

where:

$$c_1(x,t) = c_0 \cdot \text{erfc} \; \frac{1}{2} \frac{x}{\sqrt{\tau_1}} \qquad \text{(lattice diffusion)} \qquad (3.8)$$

and

$$c_2(x,t) = c_0 \frac{2x}{\sqrt{\tau_1 \cdot \pi}} \int_1^{\Delta} \exp\left(-\frac{1}{4} \frac{x^2}{\tau_1 \sigma}\right) \omega \; \sigma^{-3/2} \; .$$

$$\cdot \left[\exp(-X^2)/\sqrt{\pi} - X \; \text{erfc} \; X\right] d\sigma \qquad (3.9)$$

where:

$$\omega = \left[(\Delta - \sigma)/(\Delta - 1)\right]^{\frac{1}{2}}$$

$$\Delta = D_g / D_1$$

$$X = \omega^{\frac{1}{2}}(\sigma - 1)/\beta$$

$$\beta = 2a(\Delta - 1)/(D_1 t)^{\frac{1}{2}}$$

$2a$ = grain boundary width.

Numerical values of the c_2 solution show that $\Delta \lg c_2 =$ = const. $\Delta x^{6/5}$ as outlined before; furthermore for deep penetration $c_1 \approx 0$. Therefore c_1 can be obtained as the difference between the observed concentration c for small values of x and the extrapolation of c_1 obtained as a straight line fitting the linear part of the $\lg c$ versus $x^{6/5}$ (or more simply and without appreciable error: ver-

sus $x^{(*)}$) in the specimen interior.

From c_1 and relationship (3.8) the D_1 value is calculated. Then the product $D_g \cdot 2a$ is obtained by solving the relationship given by Le Claire [17]:

$$\frac{\partial \lg c_2}{\partial \left(\frac{x\beta^{-\frac{1}{2}}}{\sqrt{D_1 t}}\right)^{6/5}} = 0.72 \cdot \beta^{0.008}$$

which gives:

$$D_g \cdot 2a = 1.15 \cdot K^{-1.69} D_1^{0.485} t^{-0.515} \tag{3.9}$$

where $K = \partial \lg c_2 / \partial x^{6/5}$.

In a polycrystalline material, if the grain size is not much larger than $\sqrt{D_1 t}$, the model seen above is no longer valid.

In this case the diffusion along grain boundaries has the effect to enhance the bulk migration. A similar effect occurs when the dislocations inside a crystal are consider-

---

(*) This can be easily verified. Suppose for instance that a straight line $y = y_o - K x^n$ is forced to fit the experimental points in the "x^n" plot between x_1 and x_2. The extrapolated y values for $x < x_1$ will depend on n and the larger variations will be found at $x = o$, i.e. for y_o. As a typical example $y_2/y_1 = 0.1$ and $x_2/x_1 = 4$; in this case $y_o = 1.3 \cdot x_1$ for $n = 1$ and $y_o = 1.22 \cdot x_1$ for $n = 1.2$ with a difference of only 7%.

ed and the following conclusion obtained by Hart [13]
for this case can apply also to grain boundaries: the
process is described by the mathematical model seen in
the preceeding section for lattice diffusion, with the
diffusion coefficient given by:

$$D = D_l(1-f)+f \cdot D_g \qquad (3.10)$$

where f is the fraction of solute atoms within the
boundary layer.

From the above discussion it is seen that if an ex-
perimental $\lg c$ versus x (or $x^{6/5}$) curve is a straight
line, the diffusion proceeds via grain boundaries; if
however this is not observed, and the solution for lattice
diffusion fits the data (for instance the linearity between
$\lg c$ and x^2 for the instantaneous source), grain boundary
diffusion cannot be excluded unless the condition $L \gg \sqrt{D_l t}$
is verified.

c) Trapping mechanism

A trapping model has been developed by Hurst [19] and
Iwamoto [3]. Their assumptions are somewhat different
and the solutions refer to the release from slabs or cylin
ders with a uniform initial concentration.

Only qualitative comparison between the predicted and
measured xenon release from our specimens can be made at
this stage of the work, since the initial and geometrical
conditions are somewhat different from those assumed in the
model.

d) Anisotropy effects

The simple diffusion model described above in a) was developed for the isotropic case. When a body such as PyC consisting of anisotropic cristallites tilted at different angles is examined, one should consider the tensor form of the diffusion coefficients and the orientation function $I(\Phi)$ giving the density of basal planes normals per unit solid angle at an angle Φ with the axis of symmetry.

A detailed discussion of the anisotropy effect for diffusion in PyC is given in $\boxed{7}$ from which the following results are derived. The bulk diffusion coefficients $D_{/\!/}$ and $D_{\perp}$ in a direction parallel and perpendicular to the deposition planes are given by:

$$D_{\perp} = D_a \cdot \left\{ 1 - (1 - \frac{D_c}{D_a}) \cdot (1-R) \right\} \qquad (3.11)$$

$$D_{/\!/} = D_a \left\{ 1 - \frac{1}{2} (1 - \frac{D_c}{D_a}) R \right\} \qquad (3.12)$$

where:

- D_c and D_a are the coefficients of a single crystal in $< c >$ and $< a >$ direction

- R = preferred orientation parameter $\boxed{10}$

$$= \frac{\int_0^{\pi/2} I(\Phi) \sin^3 \Phi \, d\Phi}{\int_0^{\pi/2} I(\Phi) \sin \Phi \, d\Phi}$$

which is related to the BAF by the relationship:

$$BAF = 2(1-R)R^{-1}$$

From (3.11) and (3.12) the ratio $D_{/\!/}/D_{\perp}$ is obtained:

$$D_{/\!/}/D_{\perp} = \frac{1}{2}\ \frac{2-R}{R} \tag{3.13}$$

$$= \frac{1}{2}\ (BAF + 1)$$

in the hypothesis $D_c \ll D_a$.

4. Results

4.1. Xenon

Annealing times for xenon were of the order of 6 hours and some typical experimental curves giving the escaped frac tion as a function of the square root of diffusion time are plotted in Fig. 5.

These curves show two components: the first is the familiar "burst" which has always been observed in these experiments; the second is linear with $\sqrt{t}$ as predicted by eq.(3.5). Therefore the slope of this component is used to deduce a D value.

The D and burst values f_B are listed in Table II for each examined sample.

The symbol "W" after the sample number means that the face of the disk has been worked before irradiation as described above in order to obtain a flat surface whilst in the other cases the specimen has been irradiated as received. The xenon release depends on the state of the surface,

as shown in Table II: for samples S38, A 1 and A 3
the release on worked disks is greater than that on "as
received" specimens and the opposite effect is observed for
sample S16.

Arrhenius plots of the diffusion constant are shown in
Figs. 6 and 7 and the resulting activation energies and
D_O fitting the data $D(T) = D_O \cdot e^{-Q/RT}$ are shown in Table II.

The error of Q is evaluated from the reproducibility of
data and should not exceed 15% for most of the specimens,
with a maximum value of 30% for S28 and S27. The much
greater error of D_O is about a factor 10.

4.2. Barium and zirconium

Some experimental penetration profiles are given in
Figs. 8 and 9. The concentrations are normalized in such
a way that the integral of the initial profile (dotted curve
in Fig. 9) is 1. The abscissa are the penetration distances
x or x/R where R is the range.

One may observe:

a) the release for barium is much higher than for zirconium.

b) The experimental data can be fitted by the calculated cur
ves (equation 3.1) except near the surface where an anoma-
lous high concentration is observed in some cases. The
behaviour of Fig. 9 is characteristic for all the speci-
mens: at low temperature there is an effective increase
at x = o with respect to the initial condition and at
higher temperatures (1800°C) the increase is not observed
or is very low.

c) The $\lg c$ versus x^2 plot is in most cases a straight line as predicted by eq.(3.6).

d) The D and E values calculated by the fitting procedures described previously ($\lg c$ versus x^2, $\bar{x}$ and f plot) are generally in good agreement (within 20% in most cases), but for anomalous curves of the type of that appearing in Fig. 9 at 1600°C discrepancies as high as a factor 2 may be found. In any case the reported values are the arithmetic mean of those obtained by the various methods.

Tables III and IV collect the relevant data (diffusion time, f, D, E, Q) and Arrhenius plots of the diffusion coefficients are shown in Fig. 10 and 11. Fig. 10 gives also a comparison between the barium data of the present work and those of previous studies on well oriented PyC in directions parallel and perpendicular to the deposition planes.

The error in Q are of the order of $(10 \div 30)\%$ depending on the sample and the error of D_o is at least one order of magnitude.

4.3. Cesium

The cesium diffusion has been studied only at 1600°C during a single annealing run of 100 hours. The concentration of Cs in the powder surrounding the specimens was nearly constant during the anneal ($\sim 10^{-3}$ g Cs/g C).

Some results are shown in Fig. 12. The following observations can be made:

a) the concentration c_o at x = o is not the same for all the samples, but varies from $\sim 1^o/_{oo}$ to $\sim 0.1^o/_{oo}$

b) the concentration profiles cannot be fitted by eq.(3.7) with a single exception of sample S 27, for which an apparent D = $6 \cdot 10^{-11}$ cm^2/s is evaluated; in most cases there is a nearly flat profile with an increase in the first layer near the surface.

An analysis based on the grain boundary diffusion model yelds D_1 (lattice diffusion constant) $\sim 2 \cdot 10^{-13} \frac{cm^2}{s}$ for samples S 36 and B 1. The other curves do not permit analysis of the data, although, as observed before, a qualitative indication of the migration properties is obtained.

5. Discussion

The experimental results of the present study show that:

a) In the range of investigated temperatures (1200°C to 1800°C) the concentration profiles or the release curves are strongly dependent on the PyC type.

b) The diffusion behaviour cannot be fully described by a simple diffusion/evaporation model based on Fick's law, on the appropriate boundary conditions and applied to a homogeneous material. Therefore the obtained D and E values which fit the experimental data probably are not the best physical properties to be correlated with structural parameters.

c) In fact when the D values of different samples at specified temperatures are compared, no definite correlation can be found with the usual structural parameters ($c_{\frac{1}{2}}$, density, L_c, BAF).

These points are discussed separately in more detail below.

5.1. Anomalies in the diffusion curves

For xenon it has been observed that at short times the released fraction f has a burst which is usual in this type of experiments. Several explanations have been given for the burst occuring in the release from various matrices and the common assumption is to consider the burst as a surface effect; the linear part of f versus $\sqrt{t}$ therefore is characteristic of diffusion within the matrix.

A different conclusion is obtained from the findings of Yaijma and Iwamoto for Xe release from graphite. Using a trap model and the assumption that Xe atoms can diffuse rather easily within the laminar space in a graphite crystal, these authors conclude that in a isothermal annealing the transient initial fast release is characteristic of diffusion and the following slow release is controlled by the escape from traps.

This trap model apparently does not describe our results, because it predicts a linear relationship of (1-f) versus lg t at long times whilst in our case during the slow release f is proportional to $\sqrt{t}$. It must be considered that the geometrical size of our specimens are much larger than those used by Iwamoto and the released fraction are correspondingly lower. The model cannot therefore be rejected because it is possible that the release curve attains the predicted behaviour at longer times (or higher release).

Another trap model developed by Hurst contains two adjustable parameters (probability of trapping and of escape from the traps) in addition to the D value.

In this case it would be possible to find a set of parameters fitting the release curves, but only higher releases could provide a full confirmation of the theory.

The discrepancies between simple diffusion theory and experiment for solid fission products are the high concentration near the surface and the linearity of some profiles in a lg c versus x plot.

At least two effects could explain this behaviour:

- the formation of a rather stable compound near the surface, which might be decomposed at high temperature (see Fig. 9)

- the grain boundary and lattice diffusion mechanism, which
  is supported by some of the Cs results (also some Zr curves
  might equally be fitted by a straight line in a lg c ver-
  sus x or x^2 plot).

Both effects are not unexpected since some reaction could
occur near the surface and grain boundary diffusion is usual
in polycrystalline materials. Solubility effects on the con
trary should not affect the Zr and Ba curves because the con
centration is extremely low.

5.2. Correlation with structure

As said above any correlation of the results with the
structural parameters should be based on the true diffusion
constants (not the apparent values).

The diffusion mechanism in PyC is discussed in detail in
[7] [8] [9] for actinide elements and little can be added from
the present results to the conclusion that probably defects
existing at crystallite boundaries govern the transport of
solute atoms.

Some observations can however be made, based on the appa-
rent values reported in Sect. 4.

A first observation concerns the comparison of the present
results with those of [4] and [6] which were obtained in
well oriented PyC.

Table V collects the data measured at 1600°C for Ba and Xe.

It is clear that the effect of the preferred orientation is
much stronger than predicted by eq. (3.11) and (3.12).

Similar conclusions have been reported by Evans $\underline{/9/}$ and it appears that the approach followed in Sect. 3.d is not adequate to describe the anisotropy effects on atomic transport in PyC.

Excellent agreement is found between the activation energy $Q_\perp$ of the present work and that from $\underline{/6/}$ for Ba (and, incidentally, between $\underline{/4/}$ and $\underline{/6/}$ for parallel diffusion). The exception of the low density sample S 16 might be explained by some effect correlated with the porosity. This result is somewhat surprising, because in a nearly isotropic PyC the tran sport should occur mainly in the $<$ a $>$ direction of the crystal-lites, and therefore the activation energy should be near the value $Q_{/\!/}$.

For Xe a similar comparison cannot be made, because the activation energies of this work are spread in a rather wide range of values.

The second observation concerns the density effect: only for Ba and Cs there is some indication that lower density pyrocar-bons have higher diffusion coefficients (Ba) or higher concentration values (Cs), although a correlation may not be well es tablished. A similar result has been found at this Laboratory for uranium diffusion in PyC$^{(*)}$.

---

6. Conclusions

The conclusion of this work may be summarized as follows:

- nearly isotropic structures of pyrocarbon exhibit different transport properties for Ba, Xe, Zr and Cs;

- if one is interested in "apparent" diffusion constants which may fit the experimental data with a diffusion-evapo ration model, use can be made of the following diffusion coefficients:

Ba $D \sim (0.2 \div 2) \cdot 10^{-8}$ cm^2/s 1400°C

Xe $D \sim (0.1 \div 3) \cdot 10^{-13}$ cm^2/s 1400°C

Zr $D \sim (0.1 \div 1) \cdot 10^{-9}$ cm^2/s 1400°C

Cs $D \gtrsim 6 \cdot 10^{-11}$ cm^2/s 1600°C

- an advanced model for transport and release should incorporate the description of compound formation at the surface, high diffusivity paths, trapping; furthermore special experiments should be designed to give a clear evidence of the different effects;

- structural characterizations should be extended to the study of the defects which are presently believed to be the cause for trapping or for enhanced diffusion, depending on the foreign atom (for example: the microvoids distribution and possibly their orientation).

Acknowledgements

A P P E N D I X

Derivation of the simplified expression for the concentration $c(x,t)$.

According to the formalism developed in Sect. 3a the concentration inside the specimen can be written as:

$$c/c_0 = \varphi(x) - 0.5\varphi(x+\varepsilon) - 0.5\varphi(x-\varepsilon) + \Psi(x) - \Psi(x+\varepsilon)$$

where:

$$
\begin{cases}
\varphi(x) = \text{erf } \dfrac{x}{2\sqrt{\tau}} \\[3mm]
\Psi(x) = e^{Fx+F^2\tau} \text{ erfc}\left(\dfrac{x}{2\sqrt{\tau}} + F\sqrt{\tau}\right) \\[3mm]
\varepsilon = R
\end{cases}
$$

Expansion is series of $\varphi(x)$ gives:

$$
\begin{cases}
\varphi(x+\varepsilon) = \varphi(x) + \varphi'(x)\varepsilon + \varphi''\dfrac{\varepsilon^2}{2!} + \ldots\ldots \\[3mm]
\varphi(x-\varepsilon) = \varphi(x) - \varphi'(x)\varepsilon + \varphi''\dfrac{\varepsilon^2}{2!} - \ldots\ldots
\end{cases}
$$

Inserting these values and those of a similar expansion of $\Psi(x)$ in c/c_0, one obtains:

$$c/c_0 = -\varphi'' \frac{\varepsilon^2}{2!} - \varphi^{IV} \frac{\varepsilon^4}{4!} - \ldots$$

$$- \Psi' \varepsilon - \Psi'' \frac{\varepsilon^2}{2!} - \Psi''' \frac{\varepsilon^3}{3!} \ldots$$

The derivatives of φ and Ψ are:

$$\varphi' = -\frac{1}{\sqrt{\pi}} e^{-x^2/4\tau} \frac{1}{\sqrt{\tau}}$$

$$\varphi'' = \frac{1}{\sqrt{\pi}} e^{-x^2/4\tau} \frac{2x}{4\tau^{3/2}}$$

$$\circ \quad \bullet \quad \circ \quad \bullet \quad \circ \quad \circ$$

$$\Psi' = F\Psi - \varphi'$$

$$\Psi'' = F^2\Psi - F\varphi' - \varphi''$$

$$\circ \quad \circ \quad \circ \quad \bullet \quad \circ \quad \circ$$

For large values of the argument Ψ can be approximated by

$$\Psi(x) \approx \frac{2\sqrt{\tau}}{\sqrt{\pi}(x+2F\tau)} e^{-x^2/4\tau}$$

which is certainly valid for

$$F\sqrt{\tau} > 1 \qquad \text{or} \qquad x > 2\sqrt{\tau} \quad .$$

In this case the exponential $e^{-x^2/4\tau}$ is common to all the terms of the expansion and the concentration may be written as:

$$c/c_0 = \frac{e^{-x^2/4\tau}}{\sqrt{\pi}} \, Q(x,F,\tau) \quad .$$

If the first six derivatives of φ and Ψ are retained, Q assumes the form:

$$Q = (\frac{1}{F\sqrt{\tau}} - \frac{2\sqrt{\tau}}{x+2F\tau}) \sum_{1}^{6} \frac{(FR)^n}{n!}$$

$$+ \frac{1}{2F^2\tau^{3/2}} (\frac{x^2}{2F\tau} - x - \frac{1}{F}) \cdot \sum_{3}^{6} \frac{(FR)^n}{n!}$$

and it can be shown that in most of the cases of interest in this study Q slowly varying with respect to the exponential term so that it may be considered constant.

The validity of this assumption has been furthermore verified from the numerical solution of the exact equation.

Bibliography

/1/ C.J. Orth, Nuclear Sci. Eng., 9, 417 (1961)

/2/ (I)   T. Nakai, S. Yajima, K. Shiba, J. Osugi, D. Shinoda,
         Bull. Chem. Soc. Japan, 33, 4 (1960)

    (II) S. Yajima, S. Ichiba, Y. Kamemoto, K. Shiba, Bull.
         Chem. Soc. Japan, 34, 4 (1961)

    (III) Ibid., 34, 5 (1961)

/3/ K. Iwamoto, J. Oishi, Journal of Nucl. Mat., 29, 3 (1969)

/4/ B. Chinaglia, M. Domenici, F. Pieragostini, H. Walther,
    Third U.N. Geneva Conf., 9, 399 (1964)

/5/ P.E. Gethard, L.R. Zumwalt, Nucl. Applications, 3, 679 (1967)

/6/ H. Suzuki, S. Kimura, M. Matsui, J. Nucl. Sci. Technology
    6 (3), 107 (1969)

/7/ J.R. Wolfe, D.R. McKenzie, R.J. Borg, J. Appl. Phys., 36,
    6, 1906 (1965)

/8/ H.K. Lonsdale, J.N. Graves, J. Appl. Phys., 38, 3620 (1967)

/9/ R.B. Evans III, J.O. Stiegler, G.M. Watson, J. Appl. Phys.,
    41, 12, 4808 (1970)

/10/ J.C. Bokros, R.J. Price, Carbon, 4, 441 (1966)

/11/ J.C. Bokros, Carbon, 3, 17 (1965)

/12/ J.C. Laul, M.V. Ramaniah, C.L. Rao, Int. J. Appl. Radiat.
     Isotopes, 17, 306 (1966)

/13/ J.C. Fisher, J. Appl. Phys., 22, 74 (151)

/14/ R.T.P. Whipple, Phil. Mag., 45, 1225 (1954)

/15/ T. Suzuoka, Trans. Jap. Inst. Metals, 2, 25 (1961) and
      J. Phys. Soc. Japan, 19, 839 (1964)

/16/ H.S. Levine, J. Mac Cullum, J. Appl. Phys., 31, 595 (1960)

/17/ A.D. Le Claire, Brit, J. Appl. Phys., 14, 351 (1963)

/18/ E. Hart, Acta Met., 5, 597 (1957)

/19/ D.G. Hurst, AECL 1550 (1962).

TABLE I

Description of PyC structures examined in this work

Sample	Deposition Temp. (°C)	Gas	Opt. Struct.	ρ (g/cm^3)	L_c (Å)	$C_\frac{1}{2}$ (Å)	BAF
S 16	1800	P	I	1.55	69	3.45	1
S 22	2200	M	C	2.09	123	3.43	4.20
S 27	2000	M	C	2.07	116	3.43	1.15
S 28	1800	M	C	1.66	69	3.44	1.07
S 33	2000	P	I	1.83	99	3.41	1.00
S 35	2100	P	I	1.97	122	3.37	1.00
S 36	2200	P	I	2.02	122	3.39	1.06
S 38	2000	P	I	1.93	120	3.41	1.00
A 1	—	—	I	2.04	115	3.430	1.05
A 2	—	—	I	2.10	139	3.427	1.20
A 3	—	—	I	2.05	134	3.439	1.12
A 4	—	—	I	1.80	100	3.437	1.05
A 5	—	—	I	1.56	68	3.444	1.10
A 6	—	—	I	2.08	147	3.433	1.30
A 7	—	—	I	1.98	103	3.430	1.12
A 8	—	—	I	2.05	134	3.427	1.30
A 9	—	—	I	2.02	118	3.435	1.10
B 1	1900	M	I	1.81	94	3.42	1.02
B 2	1350	P	I	1.98	33	3.49	1.08

P = Propane; M = Methane; C = Columnar; I = Isotropic;

ρ = Mean density

TABLE II

Xenon diffusion coefficient D. D_o and activation energy Q.

Sample	T = 1400°C			T = 1600°C			T = 1800°C			Q Kcal/mole	D_o cm²/s
	T' °C	f_B %	$10^{15}D$ cm²/s	T' °C	f_B %	$10^{14}D$ cm²/s	T' °C	f_B %	$10^{13}D$ cm²/s		
S 16 W	1405	1	2.8	1610	0.5	6.8	1815	1	3.6	81	$1 \cdot 10^{-5}$
S 16				1605	1.35	21					
S 22 W	1400	0.47	3.5				1810	0.08	4.7	81	$1 \cdot 10^{-5}$
S 27 W	1400	0.49	110	1600	0.67	28	1810	0.20	14	42	$4 \cdot 10^{-8}$
S 28 W	1410	0.06	0.4	1600	1.23	3.1	1830	1.54	4.1	100	$1 \cdot 10^{-2}$
				1600	0.19	4.6	1830	0.49	1.8		
							1830	1.70	3.1		
S 33 W	1405	1.23	11	1600	1.6	10	1820	2	5.3	55	$4 \cdot 10^{-7}$
	1405	1.0	24				1810	3.7	4.4		
S 35 W	1410	1	8.5	1605	1.0	4.7				54	$1 \cdot 10^{-7}$
S 36 W	1410	1.35	8.8	1610	2.1	13				78	$2 \cdot 10^{-4}$
S 38 W	1400	1.23	6.7	1605	1.2	10	1810	3.7	4	65	$4 \cdot 10^{-6}$
S 38				1605	0.5	0.9					
A 1				1600	0.31	0.7	1800	0.7	0.6	94	$3 \cdot 10^{-4}$
				1605	0.47	0.3					
A 1 w				1605	2.7	2					
A 2							1800	9.1	3		
A 3				1600	0.46	1.4	1800	2.35	1	73	$5 \cdot 10^{-6}$
				1605	0.80	0.85					
A 3 w				1605	1.6	2.0					
A 4				1600	0.23	5.9					
A 5							1800	1	0.5		
A 6							1800	6.3	1.1		
A 7							1800	1.5	2.0		
A 8				1600	1	1.7					
A 9				1600	0.54	0.48					
B 1	1408	0.8	2.3	1620	0.6	2.4	1810	1.35	1.5	70	$4 \cdot 10^{-6}$
B 2	1400	1.3	11	1606	1.5	7.2	1820	2.4	3.7	57	$3 \cdot 10^{-7}$

T' = Effective temperature during annealing.

f_B = Fraction of activity released during the initial burst.

TABLE III

Barium diffusion (D) and evaporation (E) coefficients, D_0 and activation energy Q.

Sample	R (μm)	T = 1600°C				T = 1400°C				T = 1200°C				Q Kcal/mole	D_0 cm²/s
		t (min)	f (%)	$10^8 D$ cm²/s	$10^5 E$ cm/s	t (min)	f (%)	$10^9 D$ cm²/s	$10^6 E$ cm/s	t (min)	f (%)	$10^{10} D$ cm²/s	$10^8 E$ cm/s		
S 16	14	5	17	10	0.4	41	34	20	1.3	170	4	43	2.5	44	10^{-2}
						20	24	22	1.3						
S 28	13	12	60	2.3	1	20	57	3	1.6					70	10
S 33	12					20	65	17	6.8						
S 35	11	12	66	1	0.8										
S 36	11	12	67	3	1.2	45	48	2	0.8					80	50
S 38	11	5	63	7.7	2.5	41	75	5	5.5	170	1	2	0.2	83	300
A 1	11					45	74	10	3						
A 3	11					45	87	4.7	7						
B 1	12					41	74	12.5	3.5	170	9	4.7	2.6	83	600
						45	71	7.5	2.5						
B 2	11					45	<4	3.3	<0.2						

TABLE IV

Zirconium diffusion coefficient D, D_o and $Q^{(*)}$

Sample	D (cm^2/s)			Q $\frac{Kcal}{mole}$	D_o $\frac{cm^2}{s}$
	1400°C	1600°C	1800°C		
S 16		$1 \cdot 10^{-10}$	$4 \cdot 10^{-10}$	60	10^{-3}
S 27	$4.2 \cdot 10^{-11}$		$5.3 \cdot 10^{-10}$	42	10^{-5}
S 28		$2.9 \cdot 10^{-10}$	$6.7 \cdot 10^{-10}$	31	10^{-6}
		$2.2 \cdot 10^{-10}$	$5.5 \cdot 10^{-10}$		
S 33	$7.3 \cdot 10^{-11}$	$5.3 \cdot 10^{-10}$	$3.2 \cdot 10^{-9}$	60	10^{-2}
			$2.1 \cdot 10^{-9}$		
S 35		$3 \cdot 10^{-10}$			
S 36$^{(**)}$		$4 \cdot 10^{-10}$	$7 \cdot 10^{-9}$		
S 38		$3 \cdot 10^{-10}$	$7 \cdot 10^{-10}$	31	10^{-6}
B 1		$9 \cdot 10^{-10}$	$2 \cdot 10^{-9}$	30	$4 \cdot 10^{-6}$
B 2		$5 \cdot 10^{-10}$	$1.1 \cdot 10^{-9}$	32	$3 \cdot 10^{-6}$
A 3		$4 \cdot 10^{-9}$			

(*)   E values not reported; $E/D \lesssim 10$.

(**)   Irregular curves;   the D values are affected by a more
than factor 2 error;   Q and D_o have not been calculated.

TABLE V

Collection of the data measured at 1600°C for Ba and Xe

Reference	Direction	BAF	Ba		Xe	
			D $\frac{cm^2}{s}$	Q $\frac{Kcal}{mole}$	D $\frac{cm^2}{s}$	Q $\frac{Kcal}{mole}$
4	//	~ 10	$2.7 \cdot 10^{-6}$	43	10^{-10}	40
4	//	~ 30	$1.1 \cdot 10^{-5}$		$3.4 \cdot 10^{-10}$	–
4	//	~ 60	$1.1 \cdot 10^{-4}$		$5.1 \cdot 10^{-9}$	–
6	//	Not reported	$\sim 2 \cdot 10^{-5}$	47	–	–
6	$\perp$	" "	$\sim 4 \cdot 10^{-6}$	87	–	–
This work	$\perp$	$1 \div 2$	$(1 \div 10) \cdot 10^{-8}$	$\sim (80)$	$(0.1 \div 3) \cdot 10^{-13}$	$\sim (40\text{-}100)$

Sample S28
400 x
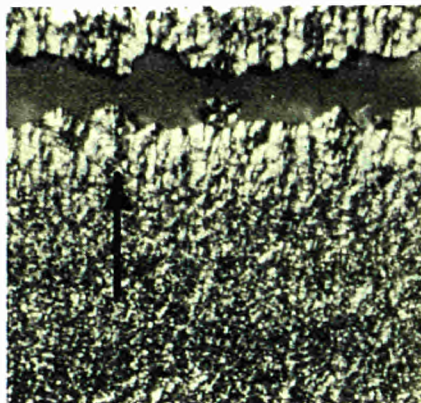
Sample S36
400 x
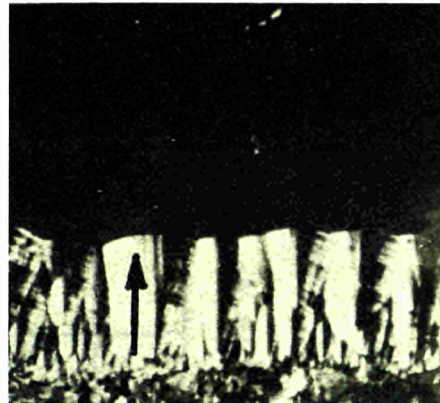
Sample S22
200 x
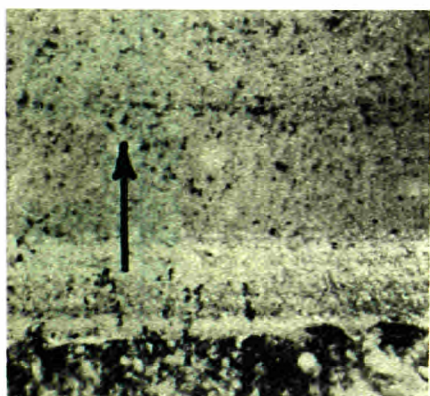
Sample S16
400 x
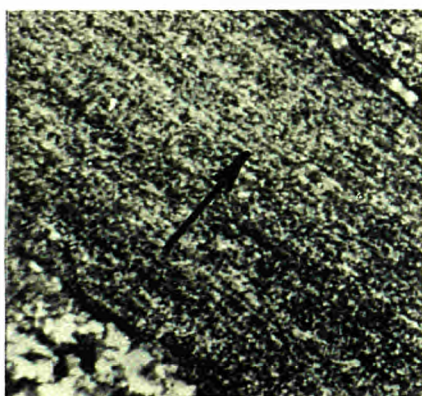
Sample A3
400 x
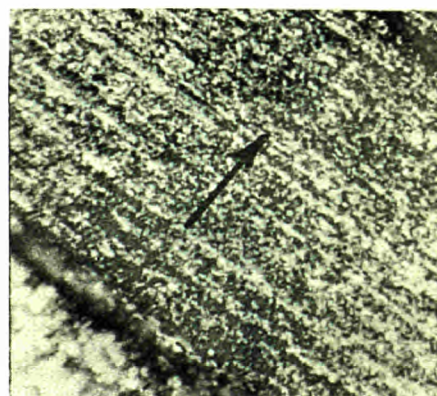
Sample A1
400 x

Fig. 1 Typical pyrocarbon structures examined in this work.
Growth direction indicated by arrows.
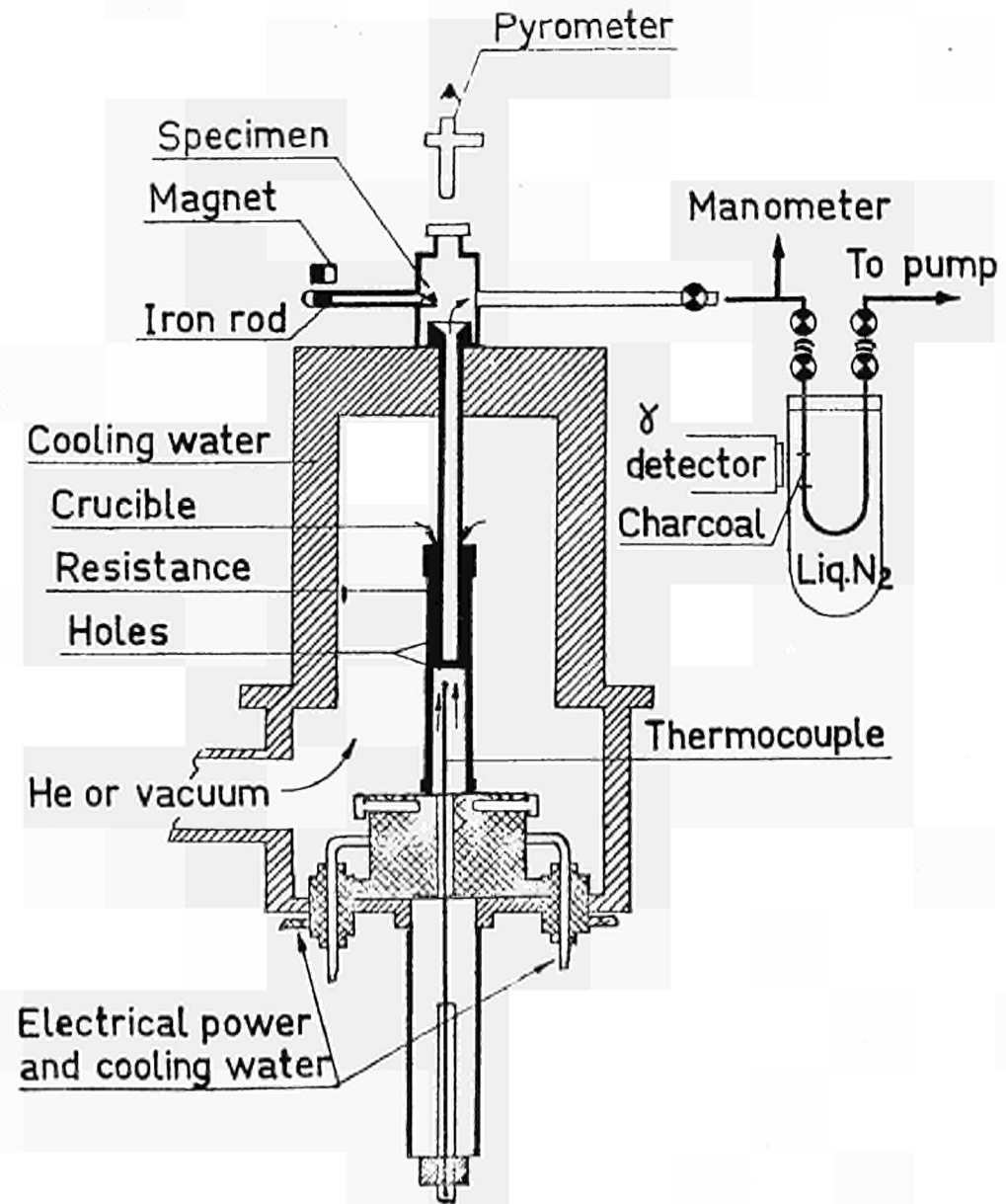
Fig. 2 - Experimental set up for annealing and measurement of xenon release.
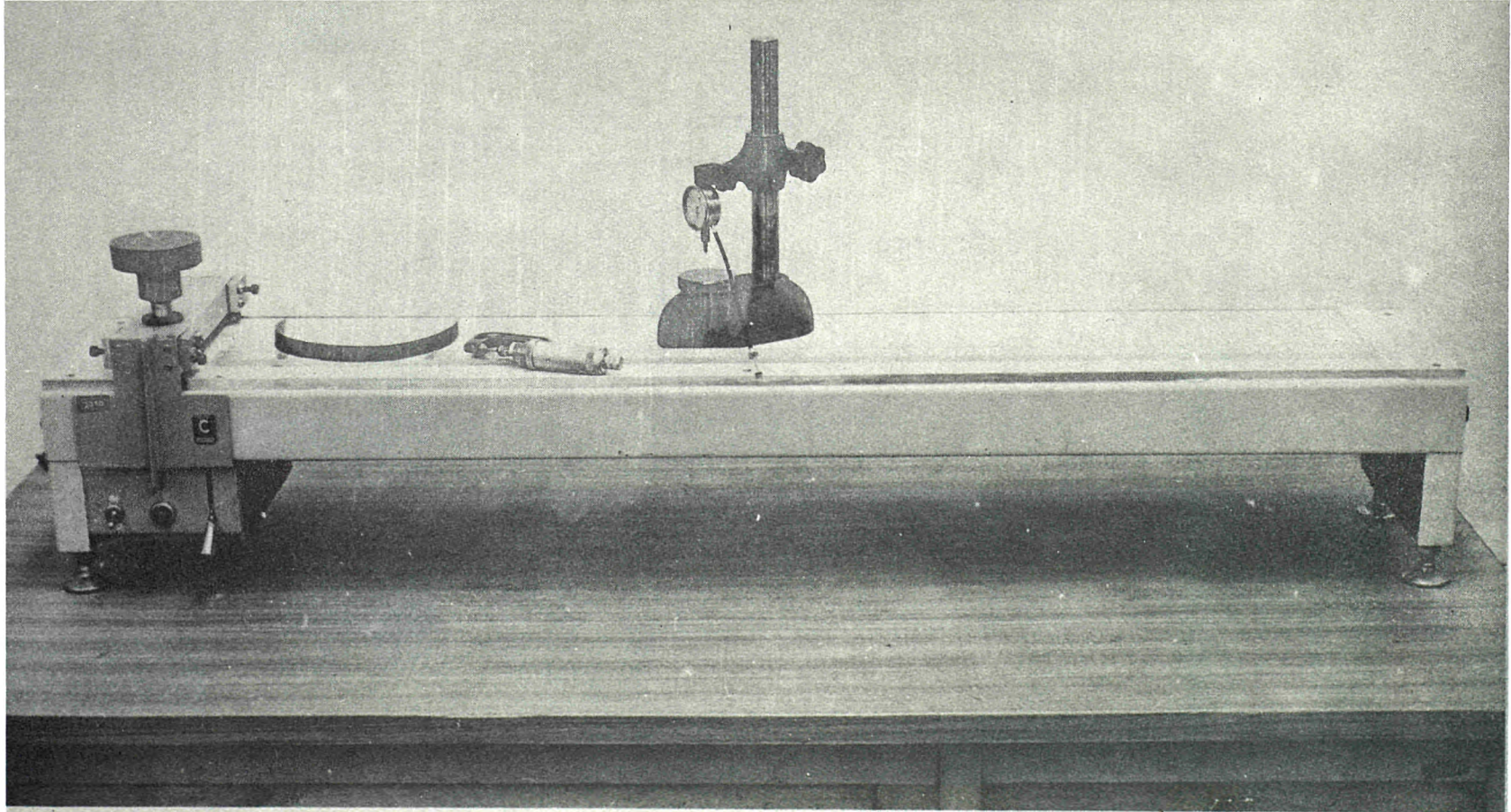
Fig. 3 - Photograph of the lapping device used for sectioning samples.
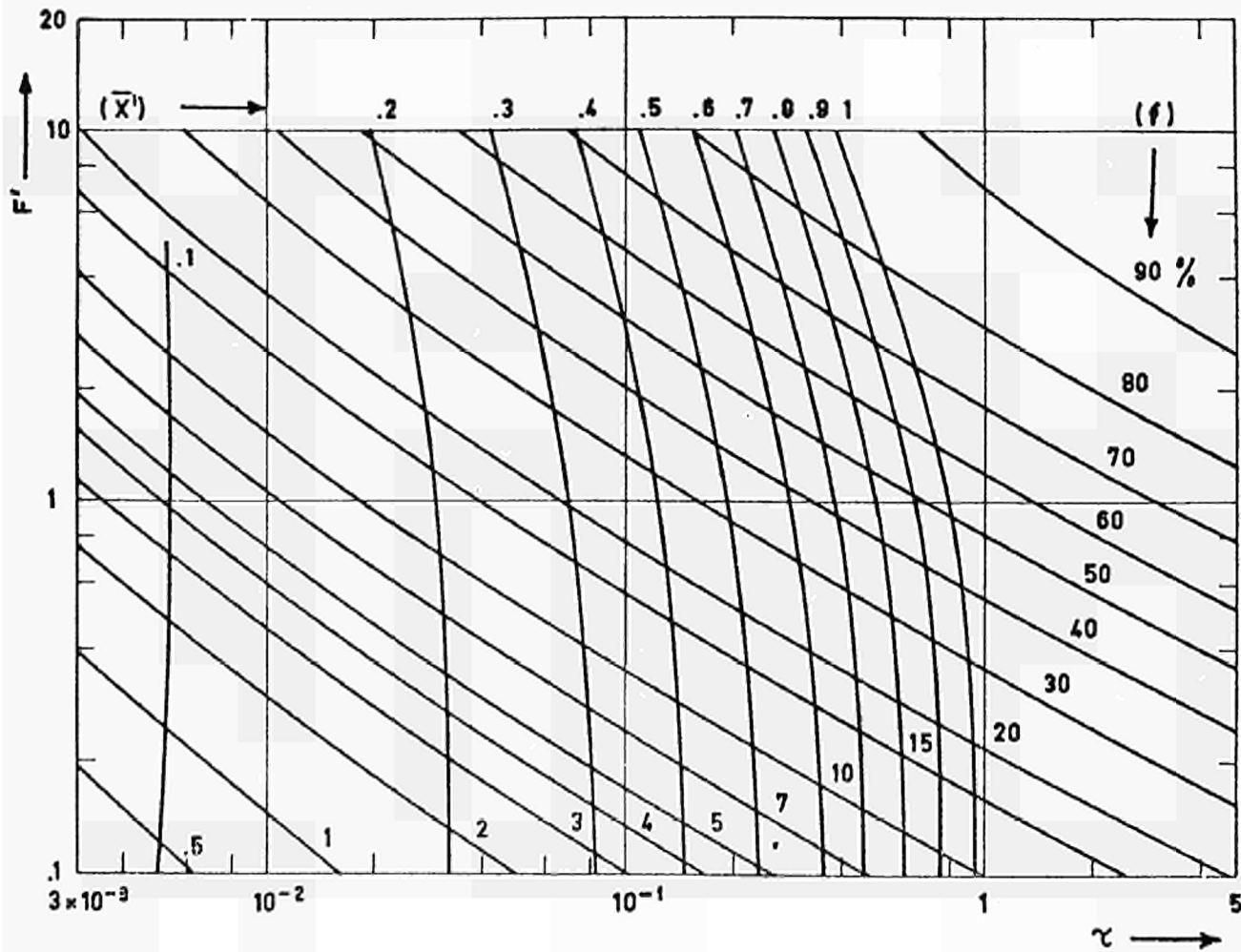
Fig. 4 -- Evaporation parameter $F' = \dfrac{Ea}{D}$ as a function of $\tau = Dt/a^2$ with $a = 10$ R at constant fraction escaped f or at constant mean penetration $\bar{x}' = \bar{x}/a$.
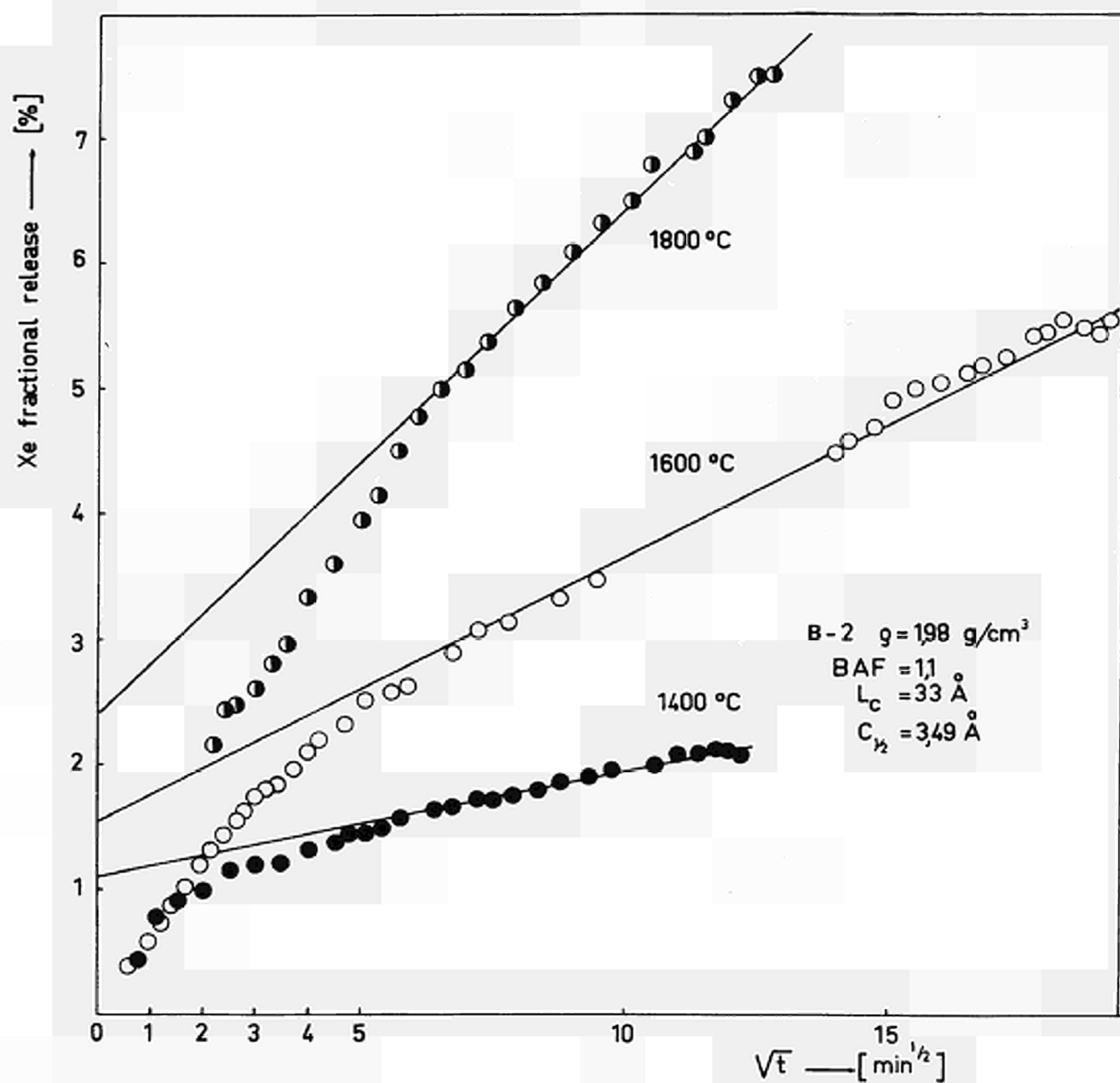
FIG. 5 XENON FRACTIONAL RELEASE AS A FUNCTION OF THE
SQUARE ROOT OF THE ANNEALING TIME.
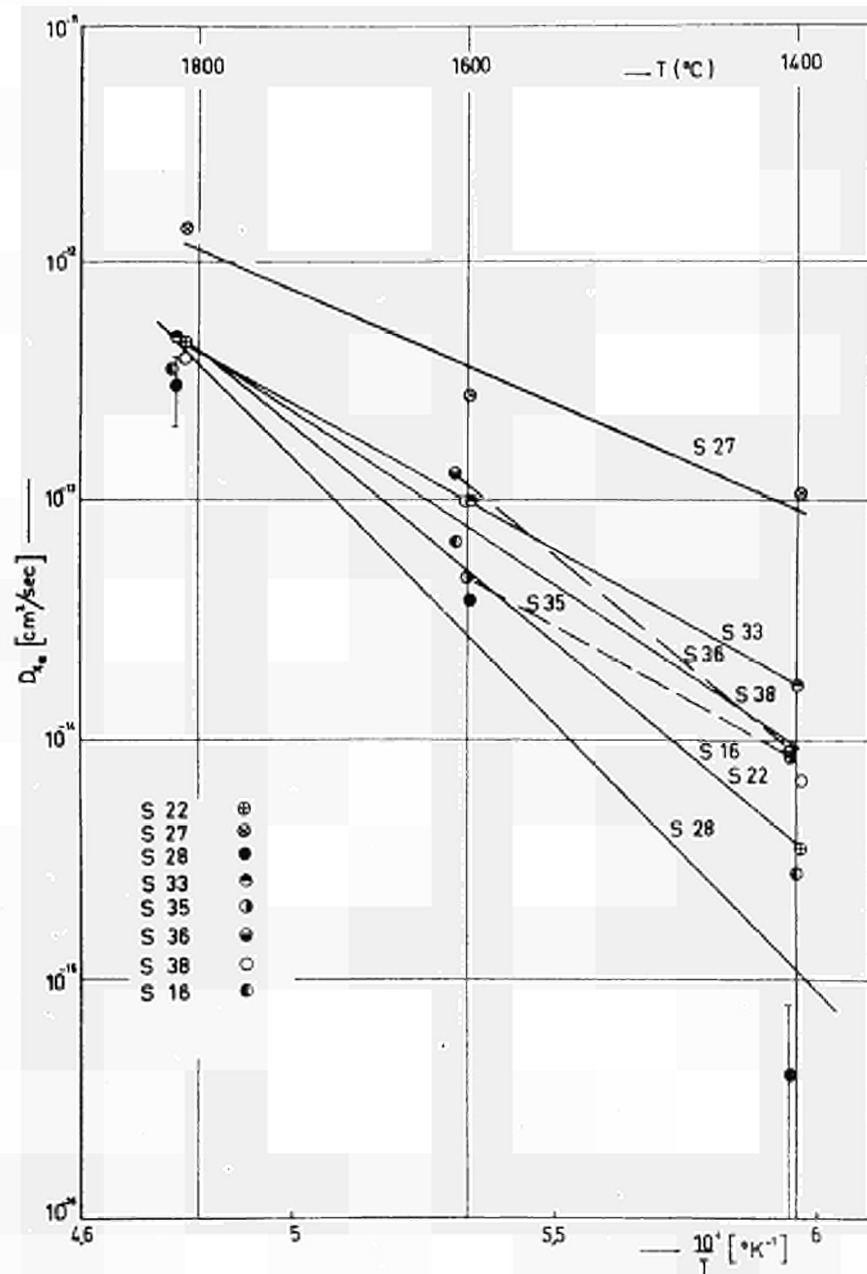
FIG. 6 ARRHENIUS PLOT OF XENON DIFFUSION COEFFICIENTS: S SAMPLES.
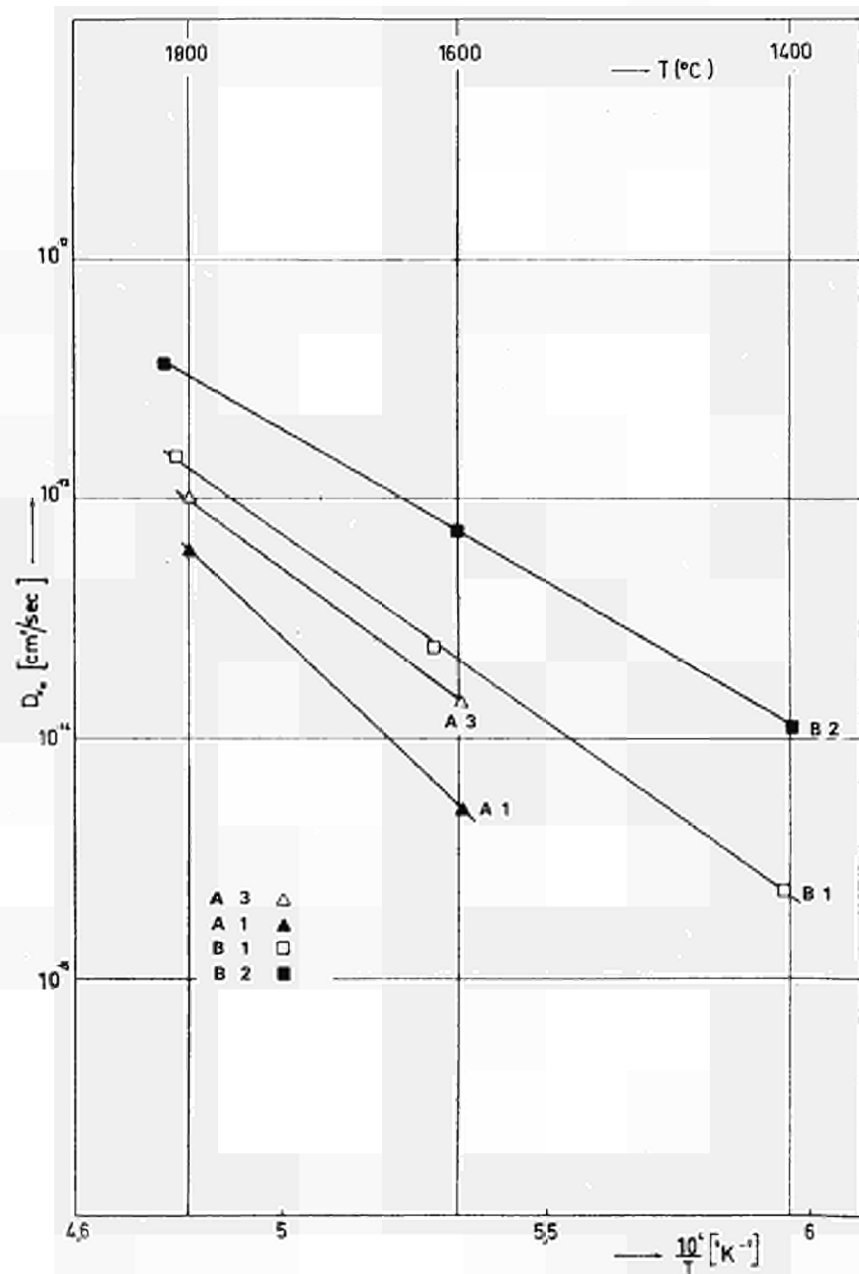
FIG. 7 ARRHENIUS PLOT OF XENON DIFFUSION COEFFICIENTS: A AND B SAMPLES.
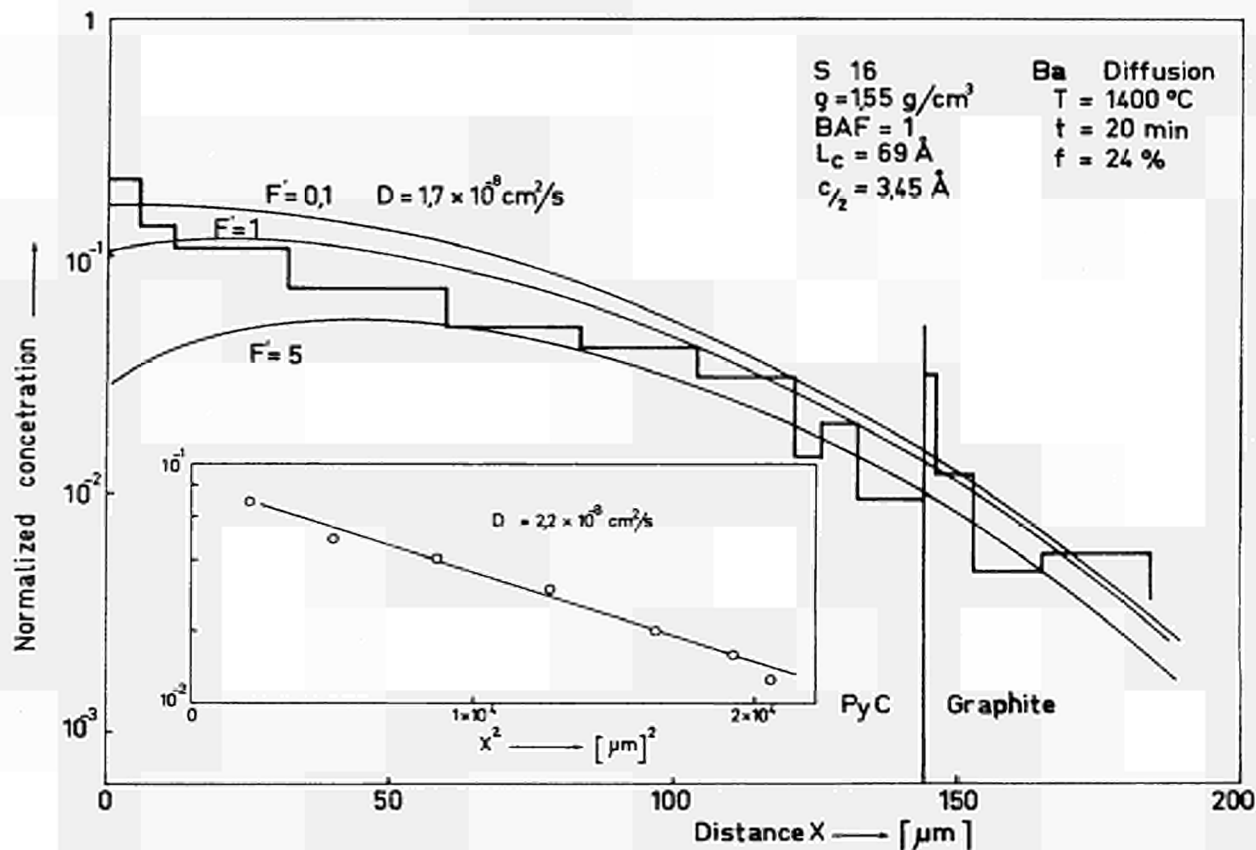
FIG. 8 CONCENTRATION PROFILE OF BARIUM. THE HISTOGRAM REPRESENTS THE EXPERIMENTAL DATA WHICH ARE FITTED BY CALCULATED CURVES WITH INDICATED D AND F' = F·10 R VALUES. IN THE INSERT THE LINEAR FITTING IN a x^2 PLOT IS SHOWN.
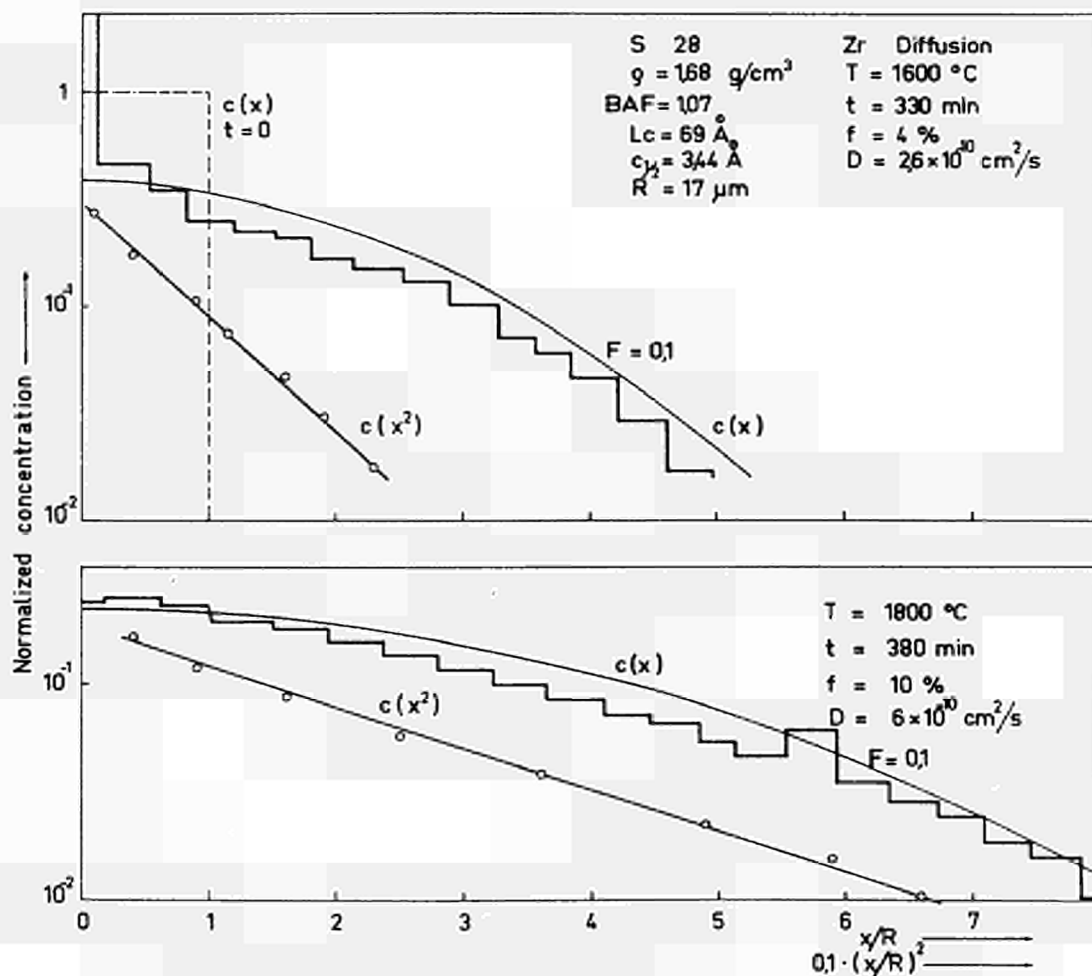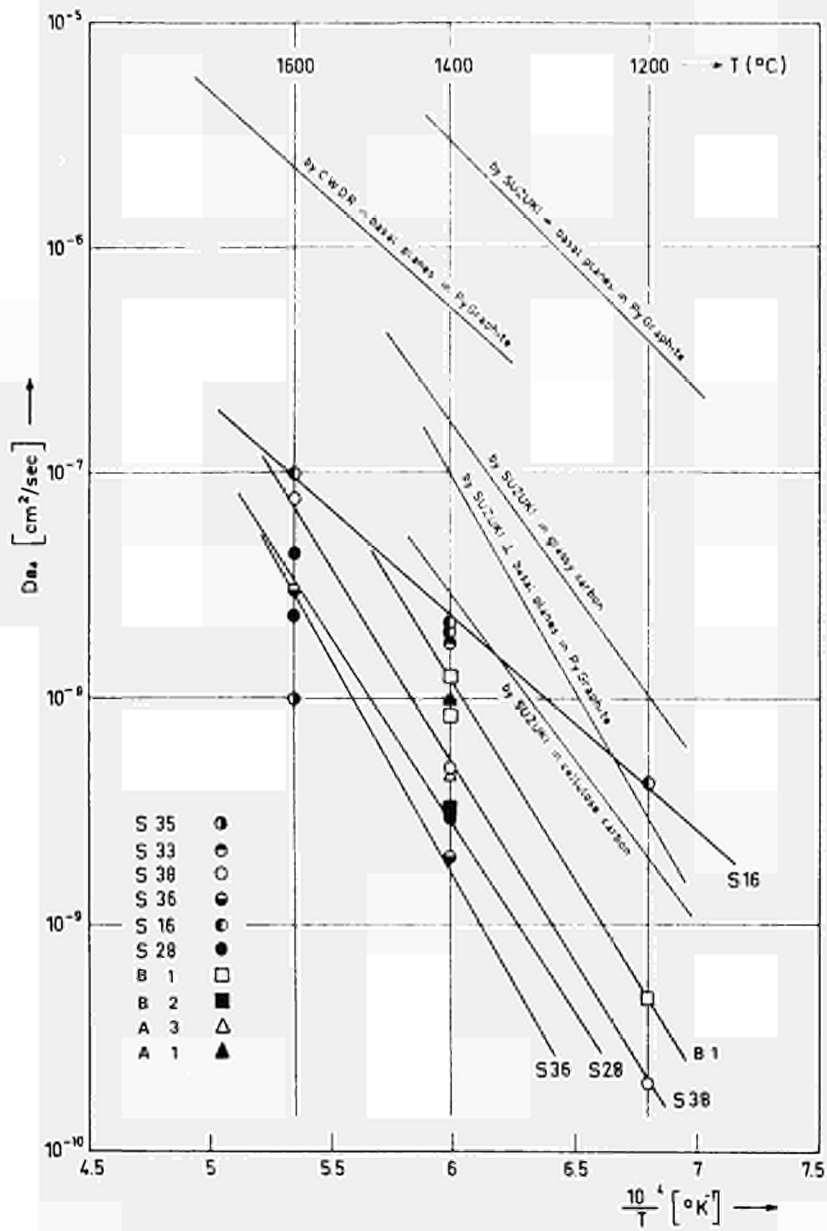

FIG. 9 CONCENTRATION PROFILES OF ZIRCONIUM. THE HISTOGRAM REPRESENTS THE EXPERIMENTAL DATA WHICH ARE FITTED, BY CALCULATED CURVES WITH INDICATED D AND F' = F·10 R VALUES. THE LINEAR FITTING IN a x^2 PLOT IS ALSO SHOWN.

FIG. 10 ARRHENIUS PLOT OF BARIUM DIFFUSION COEFFICIENTS
OF THE PRESENT WORK AND OF PREVIOUS DATA OF
SUZUKI [6] AND CHINAGLIA ET AL. [4]
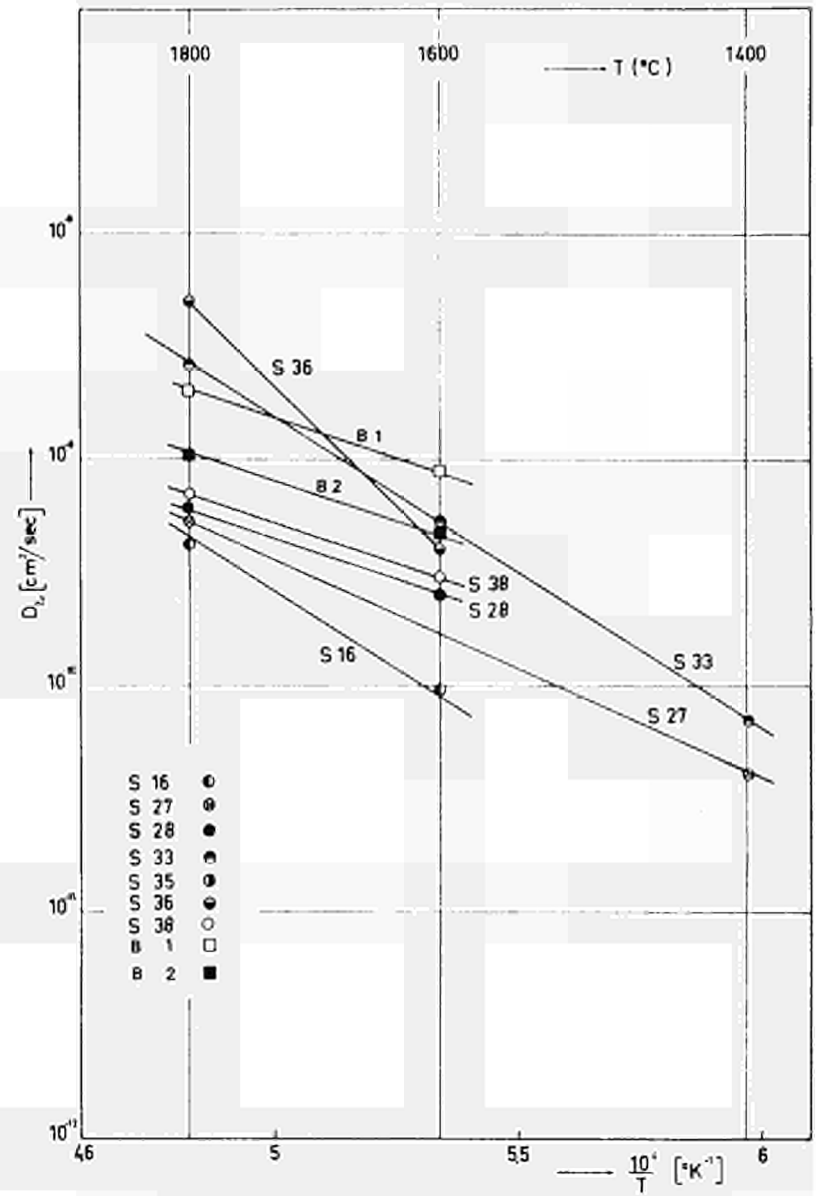
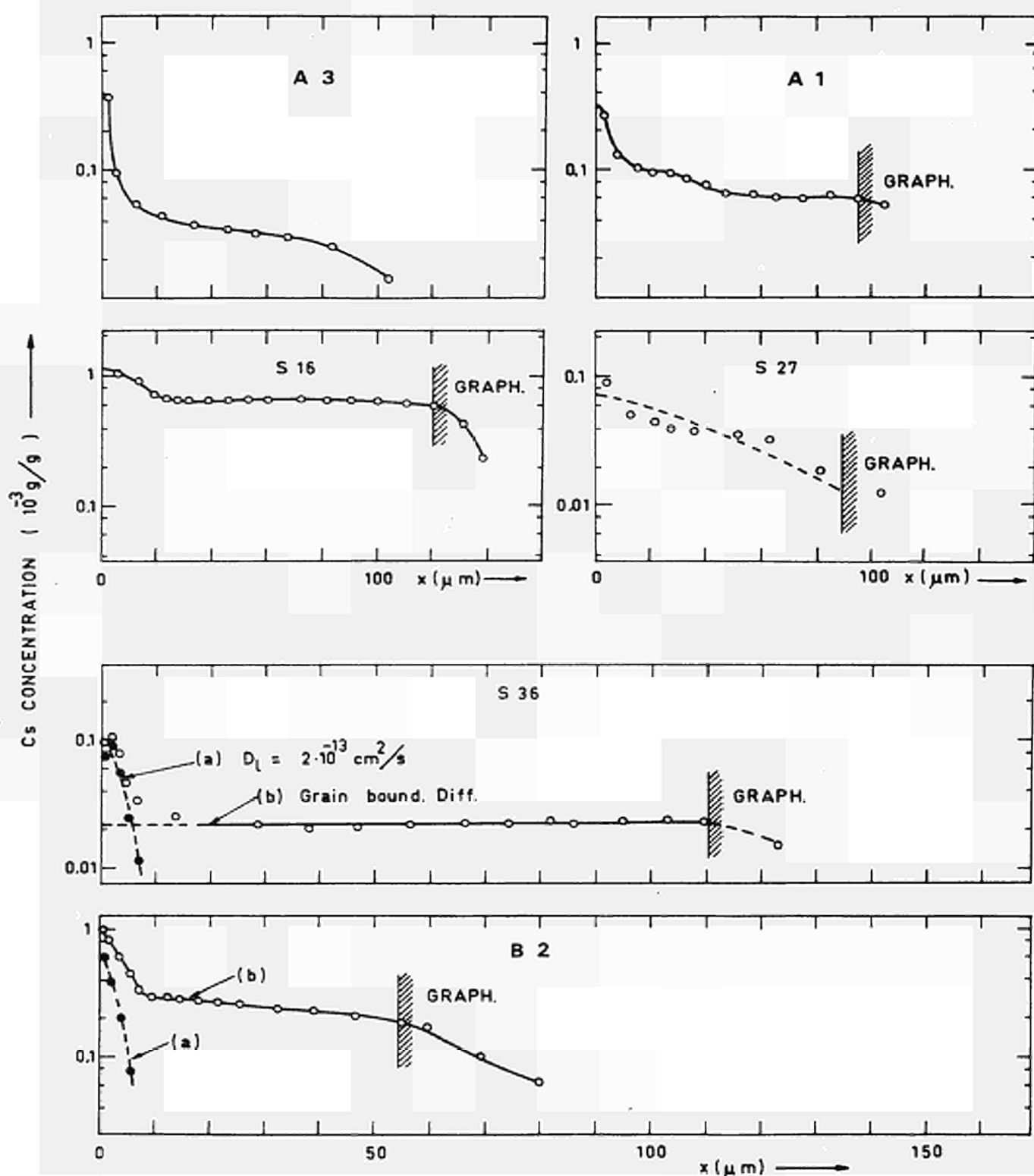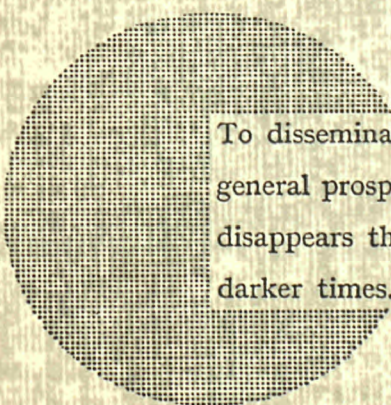FIG. 11 ARRHENIUS PLOT OF ZIRCONIUM DIFFUSION COEFFICIENTS

FIG. 12 CONCENTRATION PROFILES FOR CESIUM, CONSTANT POTENTIAL SOURCE. DOTTED LINES: FITTING CURVES BASED ON SIMPLE (SAMPLE S27) AND ON GRAIN BOUNDARY DIFFUSION (S 36, B2).

To disseminate knowledge is to disseminate prosperity — I mean general prosperity and not individual riches — and with prosperity disappears the greater part of the evil which is our heritage from darker times.

Alfred Nobel

SALES OFFICES

The Office for Official Publications sells all documents published by the Commission of the European Communities at the addresses listed below, at the price given on cover. When ordering, specify clearly the exact reference and the title of the document.

UNITED KINGDOM

H.M. Stationery Office
P.O. Box 569
London S.E. 1 — Tel. 01-928 69 77, ext. 365

BELGIUM

Moniteur belge — Belgisch Staatsblad
Rue de Louvain 40-42 — Leuvenseweg 40-42
1000 Bruxelles — 1000 Brussel — Tel. 12 00 26
CCP 50-80 — Postgiro 50-80

Agency :
Librairie européenne — Europese Boekhandel
Rue de la Loi 244 — Wetstraat 244
1040 Bruxelles — 1040 Brussel

DENMARK

J.H. Schultz — Boghandel
Møntergade 19
DK 1116 København K — Tel. 14 11 95

FRANCE

*Service de vente en France des publications
des Communautés européennes — Journal officiel*
26, rue Desaix — 75 732 Paris - Cédex 15°
Tel. (1) 306 51 00 — CCP Paris 23-96

GERMANY (FR)

Verlag Bundesanzeiger
5 Köln 1 — Postfach 108 006
Tel. (0221) 21 03 48
Telex: Anzeiger Bonn 08 882 595
Postscheckkonto 834 00 Köln

GRAND DUCHY OF LUXEMBOURG

*Office for Official Publications
of the European Communities*
Case postale 1003 — Luxembourg
Tel. 4 79 41 — CCP 191-90
Compte courant bancaire: BIL 8-109/6003/200

IRELAND

Stationery Office — The Controller
Beggar's Bush
Dublin 4 — Tel. 6 54 01

ITALY

Libreria dello Stato
Piazza G. Verdi 10
00198 Roma — Tel. (6) 85 08
CCP 1/2640

NETHERLANDS

Staatsdrukkerij- en uitgeverijbedrijf
Christoffel Plantijnstraat
's-Gravenhage — Tel. (070) 81 45 11
Postgiro 42 53 00

UNITED STATES OF AMERICA

European Community Information Service
2100 M Street, N.W.
Suite 707
Washington, D.C., 20 037 — Tel. 296 51 31

SWITZERLAND

Librairie Payot
6, rue Grenus
1211 Genève — Tel. 31 89 50
CCP 12-236 Genève

SWEDEN

Librairie C.E. Fritze
2, Fredsgatan
Stockholm 16
Post Giro 193, Bank Giro 73/4015

SPAIN

Libreria Mundi-Prensa
Castello 37
Madrid 1 — Tel. 275 51 31

OTHER COUNTRIES

*Office for Official Publications
of the European Communities*
Case postale 1003 — Luxembourg
Tel. 4 79 41 — CCP 191-90
Compte courant bancaire: BIL 8-109/6003/200